Estimation of soil strength by instrumented free-fall sphere tests

J.P Morton[1], C.D O'Loughlin[2] and D.J White[3]

Words: 4123 (main body) Figures: 7 Equations: 11 References: 33.

[1]Corresponding Author,

PhD Candidate, Centre for Offshore Foundation Systems

The University of Western Australia

35 Stirling Highway, Crawley WA 6009, Perth, Australia

Phone: +61 8 6488 3974

Fax: +61 8 6488 1044

E-mail: john.morton@research.uwa.edu.au

[2]Associate Professor, Centre for Offshore Foundation Systems

The University of Western Australia

35 Stirling Highway, Crawley WA 6009, Perth, Australia

Phone: +61 8 6488 7326

Fax: +61 8 6488 1044

E-mail: conleth.oloughlin@uwa.edu.au

[3] Winthrop Professor, Centre for Offshore Foundation Systems

The University of Western Australia

35 Stirling Highway, Crawley WA 6009, Perth, Australia

Phone: +61 8 6488 3086

Fax: +61 8 6488 1044

E-mail: david.white@uwa.edu.au

Abstract

Dynamic penetration of rigid bodies into soil is a complex problem as it involves inertial effects and extreme strain rates that enhance the soil strength. The dynamic response of a sphere in soft clay is considered in this paper through field tests in which a 0.25 m diameter steel sphere was allowed to free fall in water and dynamically penetrate the underlying soft soil. The test data, which were collected in a lake and a nearshore environment, relate to sphere velocities of up to 8 m/s, reaching sphere invert embedments close to 10 diameters. An interial measurement unit located within the sphere measured the motion response of the sphere during free fall and penetration in soil. The resulting acceleration data were used within a simple framework that accounts for both geotechnical shearing resistance and fluid mechanics inertial drag resistance, but cast in terms of a single capacity factor that can be expressed in terms of the non-Newtonian Reynolds number. The merit of the framework is demonstrated by using it as a forward model in a series of inverse analyses that calculate the undrained shear strength profile from acceleration data measured in free-fall sphere tests. The good match between these profiles and those obtained from 'push-in' piezoball penetrometer tests point to the potential for an instrumented free-fall sphere to be used a tool for charcterising the near surface strength of soft seabeds.

Keywords:

Sphere, clay, free-fall, dynamic, fluid drag, offshore, strain-rates.

Introduction

Geotechnical aspects of offshore and near-shore infrastructure projects often involve the assesment of complex soil-structure interactions involving strain rates than are often several orders of magnitude higher than those associated with laboratory element tests. The most extreme examples relate to dynamic impact events such as submarine landslide runout on pipelines and installation of free-fall projectiles such as soil samplers, penetrometers for soil strength estimation and dynamically installed anchors.

Such problems require an assessment of the net dynamic penetration resistance, which can generally be resolved into two separate components. The first is the strain-rate dependant geotechnical component (comprising the bearing resistance and for slender projectiles, frictional resistance) which represents the strength-dominated domain, and the second is the fluid dynamics component, which is the drag resistance that represents the inertia-dominated domain. Morton & O'Loughlin (2012) adopt this 'summation' approach to assess the net penetration resistance on a sphere, F_{resist}, as it dynamically penetrates soft soil:

$$F_{resist} = \frac{1}{2} C_D \rho A_p v^2 + N_c S_{u-op} A_p \quad (1)$$

The first term on the right-hand side of Equation 1 is the fluid dynamics inertial drag force (F_D), where C_D is the drag coefficient (dictated by object geometry and roughness), ρ is the density of the medium, A_p is the full projected area of the sphere, $\pi D^2/4$, and v is the velocity. The second term is the geotechnical bearing force (Fs_{u-op}) in which N_c is the bearing capacity factor and s_{u-op} is the strain-rate-enhanced undrained shear strength of the soil.

In other studies, only the first term of Equation 1 has been considered and the drag coefficient, C_D has been defined as a function of the non-Newtonian Reynolds number,

$Re_{non\text{-}Newtonian}$, also known as the Johnson number, (Zakeri *et al*., 2008; Zakeri, 2009; Zakeri *et al.,* 2009):

$$Re_{non-Newtonian} = \frac{\rho v^2}{\tau} \quad (2)$$

where τ is the mobilised shear stress within the flowing material, referred to hereafter as the operative shear strength, $s_{u\text{-}op}$.

When only the drag (C_D) term is used, the variation of C_D with $R_{e\text{-}non\text{-}Newtonian}$ (Equation 2) introduces an influence from the mobilised shear stress (or shear strength). However, this approach is not favoured for two reasons. Firstly, in the theoretical limit of a weightless medium, such an approach predicts zero resistance regardless of the shear stress or strength. Secondly, it also predicts zero resistance at zero velocity, meaning that an object can never reach a stationary equilibrium, which is the end point of all free fall penetrometer tests.

The influence of strain rate $\dot{\gamma}$ on the mobilised strength due to viscous effects is captured in the second term of Equation 1 by a power law relationship for the soil strength (Briaud *et al*., 1984; Biscontin & Pestana, 2001; Peuchen & Mayne, 2007; Jeong *et al*., 2009; Lehane *et al*., 2009):

$$s_{u-op} = s_{u,ref}\left(\frac{\dot{\gamma}}{\dot{\gamma}_{ref}}\right)^{\beta} \quad (3)$$

where $s_{u,ref}$ is the undrained shear strength at the reference strain rate $\dot{\gamma}_{ref}$, and β is a strain rate parameter.

However, if only the strength (N_c) term of Equation 1 is used, poor predictions are made for high speed penetration events (e.g. Georgiadis, 1991). This is because inertial drag forces are increasingly significant, as identified at shallow embedment (particularly for bluff bodies) by O'Loughlin *et al*. (2013) and Blake & O'Loughlin (2015).

Instead, a superposition approach is favoured with separate terms for the resistance associated with the self-weight of the medium and the shear stress (or strength) within the medium (Equation 1). With this hybrid relationship the total resistance can be expressed as a single bearing capacity factor, N:

$$N = \frac{F_{resist}}{s_{u-op} A_p} \quad (4)$$

where F_{resist} is the resistant force acting on the sphere given by Equation 1 (i.e. $F_{resist} = F_D + Fs_{u\text{-}op}$). It follows from Equations 1, 2 and 6 that a relationship between N and $Re_{non\text{-}Newtonian}$ may then be expressed as:

$$N = \frac{1}{2} C_D Re_{non-Newtonian} + N_c \quad (5)$$

This methodology captures the impact force of submarine slide debris on a pipeline in both numerical (Randolph & White, 2012) and experimental studies (Sahdi *et al*., 2014). The aim of this paper is to consider an analogous framework for the dynamic penetration of a sphere in soft soil, using data from free fall tests at two soft soil sites.

Bearing capacity factor

Throughout the analysis described in this paper, the sphere bearing capacity factor, N_c, is dependent on interface roughness and the dimensionless soil strength ratio, $s_u/\gamma'D$ (White *et al*., 2010; Morton *et al*., 2014), where γ' is the unit weight of the soil and D is the sphere diameter. Plasticity limit analyses provide bounds on N_c for a deeply embedded sphere that lie in the range $N_{c\text{-}deep}$ = 10.98 to 11.6 for a fully smooth sphere and $N_{c\text{-}deep}$ = 15.10 to 15.31 for a fully rough sphere (Randolph *et al*., 2000). The transition from a reduced N_c value at shallow penetration where the failure mechanism extends to the soil surface, to the limiting value for deep embedment associated with a full-flow mechanism, has recently been

investigated for a sphere over a wide range of $s_u/\gamma'D$ and can be expressed by the following power function (Morton *et al*., 2014):

$$N_c = N_{b-deep}\left(\frac{\hat{w}_{op}}{\hat{w}_{deep-op}}\right)^p \quad (6)$$

where the transitional depth at which $N_c = N_{c\text{-}deep}$ is given by

$$\hat{w}_{deep-op} = a + \left(b\frac{s_u}{\gamma' D}\right)^c + \frac{d-a}{1+[(s_u/\gamma' D)/e]^f} \quad (7)$$

and the fitting constants a = 16.3, b = 0.12, c = 1.3, d =0.52, e = 4.9, f = 1.5 and p is a function of the dimensionless strength ratio according to $p = 0.49(s_u/\gamma' D)^{-0.01}$.

Site Description and Soil Properties

The free-fall sphere tests were conducted at two sites; the first was Lough Erne which is a freshwater lake in County Fermanagh, Northern Ireland and the second was Firth of Clyde, which is located off the West coast of Scotland between the mainland and the Isle of Cumbrae. Water depths at the testing locations were 1 to 12 m at Erne and approximately 50 m at Clyde. Classification tests were conducted on bulk and tube samples retrieved from Erne and on piston samples retrieved from Clyde. The lakebed at Erne is very soft clay with moisture contents in the range 270 to 520%, typically about 1.5 times the liquid limit, and a fines fraction of 95%. The measured bulk unit weight of the Lough Erne clay is only marginally higher than water at γ = 10.8 kN/m^3. This is due to the very high proportion of diatoms that are evident from scanning electron microscopic images of the soil (Colreavy *et al*. 2012). These diatoms have an enormous capacity to hold water in the intraskeletal pore space (Tanaka & Locat, 1999). However the water that rests within this pore space is not considered to play a role in soil behaviour, and as such the measured unit weight and other index properties that are expressed in terms of the measured moisture content are not considered to be useful indicators of soil behaviour. The seabed at Clyde is also very soft, with moisture contents in the range 50 to 100 % (close to the liquid limit) and a fines fraction of 80 %. Consistency limits plot above or on the A-line on the Casagrande plasticity chart, indicating a clay of intermediate to high plasticity. The bulk unit weight increases from about γ = 14 kN/m^3 at the mudline to about γ = 18 kN/m^3 at about 3.5 m (limit of the sampling depth).

Figure 1 shows profiles of undrained shear strength, s_u, with depth derived from piezoball penetrometer tests and a combination of in situ vane tests (Erne), laboratory vane tests (Clyde) and fall cone tests (Clyde) The piezoball tests used a penetrometer with a ball diameter of 113 mm in Erne and ball diameters of 113 and 80 mm in Clyde. An exact 10:1 ratio between the ball and shaft areas was maintained for all penetration tests by using different shafts for each piezoball. A penetration rate of 20 mm/s (as is standard for cone testing) was adopted in an attempt to obtain undrained conditions during penetration. The best agreement between the piezoball profiles and the other strength measurements was obtained using $N_{c\text{-}deep} = 11.8$ for Clyde and $N_{c\text{-}deep} = 8.5$ for Erne.

Test Equipment and Testing Procedures

Instrumented Free-fall Sphere

The custom-made free-fall sphere (Figure 2a and 2c) is 250 mm in diameter and consists of two mild steel hemispheres that bolt together. An O-ring located between the two hemispheres prevents the ingress of water to protect an inertial measurement unit (IMU, described in the following section) that can be located within vertical cylindrical voids in each hemisphere. The sphere and IMU have a dry mass, m = 51.25 kg and an effective mass when submerged in fresh water of 43.07 kg. A 12 mm diameter Dyneema SK75 rope was used for deploying and recovering the sphere.

Inertial Measurement Unit

The inertial measurement unit (IMU) used in the free-fall sphere tests (shown in Figure 2b) is a fully self-contained motion logger designed to capture the motion history of free-fall projectiles. The IMU includes a 16-bit three component MEMS rate gyroscope (ITG 3200) and a 13-bit three-axis MEMS accelerometer (ADXL 345). The gyroscope has a resolution of

0.07 °/s with a measurement range of +/- 2000 °/s. The accelerometer has a resolution of 0.04 m/s^2 with a measurement range of +/-16 g. Data are logged by an mbed micro controller with an ARM processor to a 2 GB SD card at 400 Hz. Internal batteries are capable of powering the logger for up to 4 hours. In the free-fall sphere tests the IMU was contained in a watertight aluminium tube 185 mm long and 42 mm in diameter that fitted securely within the internal cylindrical void in the sphere.

The MEMS accelerometer measures both linear and gravitational acceleration (depending on the sphere orientation) in three orthogonal body-frame axes that are common to both the IMU and the sphere. In order to distinguish the sphere's linear acceleration component from the acceleration detected by the sensor, which may be slightly rotating, it is important to transform the body frame acceleration measurements to accelerations that are coincident with the Earth-fixed inertial frame using rotation matrices, described in detail by Blake *et al*. (2015a). Linear accelerations corresponding to the inertial frame z-axis (i.e. in the direction of Earth's gravity) were numerically integrated to establish the sphere velocity and displacement. Figure 3 shows a typical acceleration measurement of the sphere, from a hanging position to free falling in water, through penetration in soil, before a slight rebound due to soil elasticity (Dayal & Allen, 1973; Chow & Airey, 2010) as the sphere comes to rest. The importance of transforming the measured accelerations to the inertial frame is evident in Figure 3 as the body frame velocity is non-zero and the displacement is not constant when the sphere is at rest. For the remainder of the paper the inertial frame z-axis linear acceleration is referred to as the vertical acceleration.

Field Testing Procedure

The field testing program involved 87 tests that were carried out from a fixed pontoon or a hopper barge in Erne (Figure 2 c) and from a research and survey vessel in the Clyde. The

drop height, impact velocities and final embedments are summarised in Table 1. The sphere was released from various heights above the mudline to permit an assessment of the embedment response over a range of travelling velocities. The sphere release height in the 72 Erne tests was varied between 0 and 9.23 m, with resulting impact velocities in the range 0 to 7.9 m/s and sphere invert embedments of up to d = 2.373 m (~9.5 sphere diameters). In the 15 Clyde tests, the sphere release height was varied between 1 and 20 m, which resulted in impact velocities between 4.0 and 6.3 m/s and sphere invert embedments of up to d = 0.782 m (~ 3.13 sphere diameters). Embedment depths were established from the IMU data as described previously, with direct measurements based on mudline observations of markings on the retriveal line using a remotely operated vehicle in Clyde and a drop camera in Erne. These direct measurements were made to confirm that the analyses had not produced any gross error, as the accuracy in the mudline obervations was much lower that was possible from the IMU data.

Forces acting on a sphere during free-fall in water

The hydrodynamic forces acting on the sphere during free fall in water (i.e. before it impacts the underlying soil) are shown schematically in Figure 4 (a), which leads to the following equation that governs the motion response during free fall in water:

$$m\frac{dv}{dt} = F_{SW} - F_D - F_{AM} \quad (8)$$

where dv/dt is the vertical acceleration (t is time), m is the mass of the sphere, F_{SW} is the submerged weight of the sphere in water, F_D is the drag force introduced earlier in Equation 1. The final term on the right hand side of Equation 8 is the added mass force, $F_{AM} = \frac{dv}{dt}C_m m_{water}$ that occurs during non-stable flows where an object is accelerating or decelerating (Lamb, 1932). The added mass ($C_m m_{water}$) can be interpreted as the mass of fluid displaced by the sphere that is accelerated with the sphere, which is higher than the displaced mass, m_{water}

by an amount controlled by the added mass coefficient, C_m. Omitted from Figure 4 (a) and Equation 8 is the drag force that develops on the deployment and retrieval rope. This is intentional so that the framework (Equation 5) can be considered in terms of a single contact area, A_p, for both the geotechnical and fluid mechanics force components. The average drag resistance on the rope (modelled using a friction drag coefficient of 0.015 (Blake and O'Loughlin, 2015) and the contact area between the rope and the water/soil) never exceeded more than 2% of the total resistance.

As the vertical acceleration is measured, the evolution of the drag coefficient, C_D, during free-fall in water can be established from Equation 8. This is shown on Figure 5 for three Erne tests over a calculated range of Reynolds numbers, Re = 10^4 to 10^6 together with the empirical correlation between C_D and Re proposed by Morrison (2013), that is based on the benchmark experimental summarised by Schlichting (1955). At lower values of Re, between Re = 10^4 and 10^5 the back-figured experimental C_D is significantly higher than empirical values of C_D, and reduces rapidly with increasing Re. However, this range of Re corresponds with the start of free fall, with sphere velocities less than 0.5 m/s and free-fall displacements less than 0.02 m (0.08 diameters). A similar rapid variation in C_D has been associated with the hydrodynamic response of dynamically installed 'torpedo anchors', immediately after the onset of free fall (Fernandes *et al*., 2006). However, at Re > 10^6, when the sphere velocity is > 0.5 m/s and the free-fall displacement is typically about 0.02 m, the experimental C_D values agree well with the Morrison (2013) relationship using C_m = 0.5, which is exactly coincident with the theoretical value for a sphere (e.g. Sumer & Fredsoe, 1997, Pantaleone & Messer, 2011).

Forces acting on a sphere during dynamic penetration in soil

When the sphere impacts the mudline the geotechnical resistance must be considered. As discussed earlier, the combination of fluid mechanics and geotechnical resistance may be considered in terms of a single resistance factor, N, as given by Equation 7. The forces acting on the sphere during penetration in soil are shown schematically in Figure 4 (b), which leads to a modified form of Equation 8 that governs the motion response of the sphere in soil.

$$m\frac{dv}{dt} = F_{SS} - F_{resist} - F_{AM} \quad (9)$$

where F_{SS} is the submerged weight in soil, calculated as the product of the soil unit weight, γ, and the volume of displaced soil, V_{disp}, which is the volume of the sphere currently embedded in the soil in addition to the volume of a cavity that may form in the wake of the advancing sphere. This cavity may be approximated as (for example) an inverted cone, with a depth given by Equation 5 (Morton *et al*., 2014). F_{AM} is the added mass force, $F_{AM} = \frac{dv}{dt}C_m m_{soil.}$ F_{resist} is the combined resistant force acting on the sphere given by Equation 1, $F_D + Fs_{u\text{-}op}$. The latter term requires an estimation of the operational shear strength, $s_{u\text{-}op}$, which may be calculated using Equation 3, but where the strain rates are approximated as $\dot{\gamma} = v/D$ (Hurst & Murdoch, 1991; Lehane *et al*., 2009; O'Loughlin *et al*., 2009) such that:

$$s_{u-op} = s_{u,ref}\left(\frac{(v/D)}{(v/D)_{ref}}\right)^{\beta} \quad (10)$$

where $(v/D)_{ref}$ is a proxy for the reference strain rate associated with the reference value of undrained shear strength, $s_{u,ref}$. As shown on Figure 1, the majority of the s_u measurements were made using a 113 mm diameter piezoball penetrated at 20 mm/s, so $(v/D)_{ref} = 0.18\ s^{-1}$. The added mass in Equation 9 may be calculated in the same way as for free-fall in water, using $C_m = 0.5$ but with the density, ρ, of soil rather than of water, corresponding to an added mass of 4.2 kg in Erne and 6.1 kg in Clyde.

Rearranging Equation 9 allows N to be calculated directly from the vertical acceleration measurements, as shown against $Re_{non\text{-}Newtonian}$ on Figure 6 for all the test data included in Table 1 (Erne, Figure 6a) and Table 2 (Clyde, Figure 6b). The operational strength, $s_{u\text{-}op}$,

which is reflected in both the vertical and horizontal axes of Figure 6a and 6b, was calculated using $\beta = 0.05$, which is at the lower end of the ranges $\beta = 0.05$ to 0.17 quoted by Jeong *et al*. (2009) and $\beta = 0.05$ to 0.15 quoted by O'Loughlin *et al*. (2013). $\beta = 0.05$ is consistent with a 11.5% increase in undrained shear strength for every log cycle increase in shear strain rate, and is within the 10 to 20 % range commonly reported (e.g. Vade & Campenella, 1977; Graham *et al*., 1983; Lefebvre & Leboeuf, 1987).

The breadth of the range in β quoted in the literature may be (at least in part) attributed to the order of magnitude difference between the operational strain rate and the reference strain rate used in Equation 3. The maximum v/D values associated with the free-falling sphere tests considered here is v/D = 31 s^{-1}, which is two orders of magnitude higher than $(v/D)_{ref} = 0.18$ s^{-1}. This is similar to the range in v/D associated with variable rate penetrometer and laboratory vane tests, which tend to give β values close to the lower end of the range quoted above, e.g. $\beta = 0.06$ to 0.08 (Lehane *et al*., 2009) or $\beta = 0.055$ (Biscontin & Pestana, 2001).

The upper bound on $Re_{non\text{-}Newtonian}$ in Figure 6a approaches 10^4 in Erne and over 10^2 in the Clyde. These upper bounds correspond with tests where the impact velocity was close to the terminal velocity of the sphere and are lower for Clyde due to the higher soil strength at the mudline when the sphere velocity is high. The lower bound $Re_{non\text{-}Newtonian} = 10^{-4}$ and 10^{-1} for Erne and Clyde respectively were selected to omit the final 10 mm of embedment, where the sphere velocity was typically 0.2 m/s and the back figured values of N begin to reduce suddenly, indicating that other forces (perhaps from impact of the following rope or shackle) are involved.

Figure 6 highlights that at $Re_{non\text{-}Newtonian} < \sim 3$, soil strength rather than inertial drag is the dominant form of resistance, whereas for $Re_{non\text{-}Newtonian} > \sim 3$, N increases linearly with $Re_{non\text{-}Newtonian}$ highlighting the dominance of inertial drag resistance. The annotation indicating the

normalised depth (d/D) and approximate sphere velocity in Figure 6 shows that this occurs at shallow depths where the magnitude of $s_{u\text{-}op}$ (linked to the geotechnical component) is very low and the velocity is very high. Although the sphere velocity is linked to both the geotechnical and fluid mechanics terms, the inertial drag has a much higher velocity dependency than the geotechnical term, and therefore is the dominant form of resistance at $Re_{non\text{-}Newtonian} > \sim 3$.

Also shown on Figure 6 is the theoretical response described by Equation 5, which provides a good fit to both datasets using $C_D = 0.26$, and equivalent data for a cylinder from experiments in a flume (Zakeri *et al*., 2008; Zakeri *et al*., 2011) and in a centrifuge (Sahdi *et al*., 2014). These data exhibit the same trends as for the sphere, albeit that the cylinder data plot above the sphere data at $Re_{non\text{-}Newtonian} > \sim 3$, as at high Reynolds numbers C_D for a cylinder is higher than that for a sphere (Schlichting, 1955).

At $Re_{non\text{-}Newtonian} < \sim 3$, N for the sphere occupies a wider range than for the cylinder as the sphere. This is because the sphere embedment depth is changing, reflecting the variation in N_c during shallow penetration (all cylinder tests were at a single embedment). In Erne, the sphere penetrated to (on average) between 1 and 2 m, equivalent to 4 to 8 diameters, which is sufficient in this soft soil to establish a full-flow deep failure mechanism. The approximate range of Erne N values at $Re_{non\text{-}Newtonian} < \sim 3$ is typically $N_{c\text{-}deep} = 6$ to 9.5, with an arithmetic mean of $N_{c\text{-}deep} = 7.5$, which is to be expected given that the strength data input to the analyses were determined using $N_{c\text{-}deep} = 8.5$ (as described earlier). Over the same range of at $Re_{non\text{-}Newtonian}$, Clyde N values do not reach $N_{c\text{-}deep} = 11.8$ used to interpret the piezoball data. The approximate range of Clyde N values at $Re_{non\text{-}Newtonian} < \sim 3$ is typically $N_{c\text{-}deep} = 7$ to 10, with an arithmetic mean of $N_{c\text{-}deep} = 9$. This difference to the piezoball analysis is to be expected as the final sphere embedment depth at Clyde is typically 0.65 m (2.6 sphere

diameters), which for this soil with a relatively high $s_u/\gamma'D$, is insufficient to develop a deep failure mechanism (i.e. $N_c < N_{c\text{-}deep}$).

Soil strength estimation using free-fall sphere data

The merit of the framework described in the previous section is now explored by performing a simple inverse analysis on vertical acceleration data measured during free-fall sphere tests to obtain s_u profiles for both sites. Rearranging Equation 9, the undrained shear strength, s_u, at a given depth is:

$$s_u = \frac{F_{SS} - \frac{dv}{dt}(m + C_m m_{soil})}{N A_p \left(\frac{v}{v_{ref}}\right)^{\beta}} \quad (11)$$

In Erne, a deeply embedded soil flow mechanism is assumed (as described previously), such that the buoyancy force may be calculated using the sphere volume and N may be determined using Equation 5 with $N_c = 8.5$ and $C_D = 0.26$. In Clyde the dynamic sphere penetration is relatively shallow and the dimensionless strength ratio $s_u/\gamma'D$ is relatively high (~1.8 at the final sphere embedment depth), such that both the variation in N_c with embedment depth and the cavity formed by the penetrating sphere require consideration. It is assumed here that the transitional embedment depth at which $N_c = N_{c\text{-}deep}$ may be calculated using Equation 5 and the cavity geometry is an inverted cone (Morton *et al*. 2014). This gives a transitional embedment depth at which $N_c = N_{c\text{-}deep}$ (measured to the invert of the sphere) of approximately 1.2 m. This allows the variation in N_c with depth to be determined (using Equation 6) and the inverted cone volume to be calculated. The variation in N_c is included in Equation 5 and the changing buoyancy force during penetration is calculated in Equation 11 using the current cavity geometry.

The resulting s_u profiles are compared with their piezoball counterparts in Figure 7 using operative rather than invert depth (White *et al*., 2010, Morton *et al*., 2014). The Clyde

piezoball data have been interpreted using the same shallow analysis described for the dynamic data. The excellent agreement between the 'push-in' and free-fall s_u profiles is extremely encouraging and points both to the merit of the relatively simple framework proposed, which is made possible by the simple sphere geometry, and also to the potential of the instrumented free-fall sphere as an effective tool for characterising the near-surface strength of soft seabeds.

Conclusions

Acceleration data, measured in field tests where a steel sphere was allowed to free fall through water and penetrate the underlying soft soil, have been used in the development of a theoretical framework that describes the forces acting on a sphere during dynamic embedment in soil. The framework is cast in terms of both fluid mechanics inertial drag resistance and geotechnical shear resistance, but formulated in terms of a single capacity factor that approaches the conventional bearing capacity factor at low strain rates, but may be up to two orders of magnitude higher when the sphere approaches its terminal velocity. Experimental data gathered from 87 separate free fall sphere tests at two sites are interpreted. The merit of the framework was demonstrated through a simple inverse analysis in which the undrained shear strength measured during free-fall sphere tests was calculated from the measured acceleration data, accounting for buoyancy created by the passage of the advancing sphere and a reduced bearing capacity factor at shallow embedment. The resulting undrained shear strength profiles were shown to be in excellent agreement with those derived from piezoball penetrometer tests, indicating the potential of the free-fall sphere as a simple yet effective tool for characterising the near-surface strength of soft seabeds.

Acknowledgements

This work forms part of the activities of the Centre for Offshore Foundation Systems (COFS), currently supported as a node of the Australian Research Council Centre of

Excellence for Geotechnical Science and Engineering and as a Centre of Excellence by the Lloyd's Register Foundation. The Lloyd's Register Foundation invests in science, engineering and technology for public benefit, worldwide. The third author acknowledges the support of Shell Australia via the Shell EMI Chair in Offshore Engineering at UWA.

References

Biscontin, G. & Pestana, J. M. (2001). Influence of peripheral velocity on vane shear strength of an artificial clay. *ASTM Geotechnical Testing Journal,* **24**, No. 4, 423–429.

Blake, A.P. & O'Loughlin, C.D. (2015). Installation of dynamically embedded plate anchors as assessed through field tests. *Canadian Geotechnical Journal*, in press, doi:10.1139/cgj-2014-0327.

Blake, A. P., O'Loughlin, C.D., Morton, J. P., O'Beirne, C., Gaudin, C. & White, D. J. (2015a). In-situ measurement of the dynamic penetration of free-fall projectiles in soft soils using a low cost inertial measurement unit. *ASTM Geotechnical Testing Journal* (under review).

Briaud, J. L., Garland, E. & Felio, G. Y. (1984). Rate of loading parameters for vertically loaded piles in clay. In *Proceedings of the 16th Annual Offshore Technology Conference*, Houston, Texas, USA, paper OTC 4694, 407-412.

Colreavy, C., O'Loughlin, C. D. & Ward, D. (2012). Piezoball testing in soft lake sediments. In *Proceedings of the 4th International Conference on Geotechnical and Geophysical Site Characterisation,* Pernambuco, Brazil, 597-602.

Chow, S. H. & Airey, D. W. (2010). Laboratory free falling penetrometer test into clay. In *Proceedings of the 2nd International Symposium on Frontiers in Offshore Geotechnics*, Perth, Australia, 265-270.

Dayal, U. & Allen, J. H. (1973). Instrumented impact cone penetrometer. *Canadian Geotechnical Journal* **10,** No. 3, 397–409.

Fernandes, A., de Araujo, J., de Almeida, J., Machado, R. & Matos, V. (2006). Torpedo anchor installation hydrodynamics. *Journal of Offshore Mechanics and Arctic Engineering,* **128**, 286-293.

Georgiadis, M. (1991). Landslide drag forces on pipelines, Soils and Foundations. *Japanese Society of Soil mechanics and Foundation Engineering*. **31**, No.1, 156-161.

Graham, J., Crooks, J. H. A. & Bell, A. L. (1983). Time effects on the stress-strain behaviour of natural soft clays. *Géotechnique*, **33**, No. 3. 327–340.

Hurst, R. B. & Murdoch, S. (1991). Measurement of sediment shear strength for mine impact burial predictions. *Report of the 18th Meeting of the Mines and Mine Countermeasures Technology Panel GTP-13*.

Jeong, S. W., Leroueil, S. & Locat, J. (2009). Applicability of power law for describing the rheology of soils of different origins and characteristics. *Canadian Geotechnical Journal*, **46**, 1011–1023.

Lamb, H. (1932). *Hydrodynamics*. Cambridge University Press.

Lefebvre, G. & LeBoeuf, D. (1987). Rate effects and cyclic loading of sensitive clays. *ASCE Journal of Geotechnical Engineering*, **113**, No. 5, 476–489.

Lehane, B. M., O'Loughlin, C. D., Gaudin, C. & Randolph, M. F. (2009). Rate effects on penetrometer resistance in kaolin. *Géotechnique* **59,** No. 1, 41–52.

Morrison, F. A. (2013). *An Introduction to Fluid Mechanics*. New York: Cambridge University Press.

Morton, J. P & O'Loughlin, C. D. (2012). Dynamic penetration of a sphere in clay. In *Proceedings of 7th International Offshore Site Investigation and Geotechnics Conference: Integrated Geotechnologies – Present and Future*, London, UK: Society for Underwater Technology, 223–230.

Morton, J. P., O'Loughlin, C. D. & White, D. J. (2014). Strength assessment during shallow penetration of a sphere in clay. *Géotechnique Letters* **4**, October–December, 262–266.

O'Loughlin, C. D., Richardson, M. D. & Randolph, M. F. (2009). Centrifuge Tests on Dynamically Installed Anchors. In *Proceedings of 28th International Conference on Ocean, Offshore and Arctic Engineering*, Honolulu, Hawaii, OMAE2009-80238, 391-399.

O'Loughlin, C. D., Richardson, M. D., Randolph, M. F. & Gaudin, C. (2013). Penetration of dynamically installed anchors in clay. *Géotechnique* **63**, No. 11, 909–919, http://dx.doi.org/10.1680/geot.11.P.137.

Pantaleone, J. & Messer, J. (2011). The added mass of a spherical projectile. *American Journal of Physics*, **79**, No. 12, 1202-1210.

Peuchen, J. & Mayne, P. (2007). Rate effects in vane shear testing. In *Proceedings of the 6th International Conference on Offshore Site Investigation and Geotechnics: Confronting New Challenges and Sharing Knowledge*, London, UK. 187-194.

Randolph, M. F., Martin, C. M. & Hu, Y. (2000). Limiting resistance of a spherical penetrometer in cohesive material. *Géotechnique* **50**, No. 5, 573–582, http://dx.doi.org/10.1680/geot.2000.50.5.573.

Randolph, M. F. & White, D. J. (2012). Interaction forces between pipelines and submarine slides: a geotechnical viewpoint. *Ocean Engineering*, **48**, July, 32–37.

Sahdi, F., Gaudin, C., White, D. J., Boylan, N. & Randolph, M. F. (2014). Centrifuge modelling of active slide–pipeline loading in soft clay. *Géotechnique* **64**, No. 1, 16–27, http://dx.doi.org/10.1680/geot.12.P.191.

Schlichting, H. (1955). *Boundary Layer Theory*. New York: McGraw-Hill.

Sumer, B.M. & Fredsoe, J. (1997). Hydrodynamics around cylindrical structures. *World Scientific*. Singapore.

Tanaka, H., & Locat, J. (1999). A microstructural investigation of Osaka Bay clay: the impact of microfossils on its mechanical behaviour. *Canadian Geotechnical Journal*, **36**, 493–508.

Vade Y. P. & Campanella, R. G. (1977). Time dependent behaviour of undisturbed clay. *ASCE Journal of Geotechnical Engineering*, **7**, No. 2, 693–709.

White, D. J., Gaudin, C., Boylan, N. & Zhou, H. (2010). Interpretation of T-bar penetrometer tests at shallow embedment and in very soft soil. *Canadian Geotechnical Journal*, **47,** No. 2, 218-229.

Zakeri, A., Hoeg, K. & Nadim, F. (2008). Submarine debris flow impact on pipelines – Part I: Experimental investigation. *Coastal Engineering*, **55**, No. 12, 1209–1218.

Zakeri, A., Hoeg, K. & Nadim, F. (2009). Submarine debris flow impact on pipelines – Part II: Numerical analysis. *Coastal Engineering*, **56**, No. 1, 1–10.

Zakeri, A., Chi, K. & Hawlader, B. (2011). Centrifuge modelling of glide block and out-runner block impact on submarine pipelines. In *Proceedings of the Offshore Technology Conference*, Houston, Texas, USA, paper OTC 21256.

List of Tables:

List of Figures:

Table 1. Free-fall sphere test data from the Erne tests

Test no.	Release height (m)	Impact velocity (m/s)	Sphere invert embedment depth (m)
1	0.50	2.69	1.017
2	0.50	0.01	1.115
3	0.50	2.79	1.150
4	1.00	4.01	1.439
5	1.00	3.87	1.595
6	1.00	3.89	1.500
7	1.00	3.88	1.484
8	3.00	5.79	2.378
9	4.00	6.63	2.055
10	5.00	6.80	2.152
11	2.00	5.25	1.841
12	3.00	6.15	1.974
13	1.00	3.74	1.097
14	0.50	2.46	1.128
15	1.00	2.46	1.128
16	2.00	5.22	1.855
17	3.00	6.11	1.846
18	3.00	6.44	2.117
19	0.50	2.64	1.243
20	1.00	3.80	1.295
21	1.66	5.19	1.572
22	3.00	6.20	1.995
23	0.44	2.58	1.088
24	0.54	2.81	1.116
25	0.61	2.97	1.148
26	0.50	2.72	1.148
27	0.02	0.55	1.192
28	1.04	3.94	1.308
29	1.07	3.93	1.303
30	2.13	5.38	1.718
31	1.82	5.23	1.620
32	2.22	5.70	1.456
33	2.00	4.86	1.613
34	2.62	6.15	1.732
35	2.55	6.30	1.956
36	2.84	6.35	1.804
37	2.61	6.51	1.788
38	2.47	6.14	1.803
39	3.39	6.63	1.889
40	0.50	2.67	0.918

41	0.84	3.68	1.183
42	1.85	5.34	1.543
43	2.00	5.35	1.518
44	3.00	6.19	1.747
45	2.81	6.43	1.766
46	0.00	0.00	0.791
47	0.00	0.00	0.732
48	0.00	0.00	0.646
49	3.00	6.31	1.815
50	3.00	6.45	1.780
51	3.31	6.58	1.878
52	0.00	0.00	0.889
53	0.00	1.32	0.903
54	0.00	0.00	0.748
55	1.00	3.86	1.392
56	2.00	5.06	1.491
57	3.00	6.05	1.805
58	0.00	0.00	0.754
59	1.00	3.72	1.276
60	2.00	5.09	1.588
61	3.00	5.96	1.735
62	3.93	6.60	1.972
63	4.49	6.62	2.081
64	4.73	6.75	1.964
65	8.95	7.88	2.373
66	6.28	7.41	2.181
67	4.00	6.36	1.927
68	4.00	5.97	1.732
69	3.99	6.42	1.820
70	9.27	7.47	2.127
71	6.78	7.91	2.108
72	3.70	6.78	2.052

Table 2. Free-fall sphere test data from the Clyde tests

Test no.	**Release height (m)**	**Impact velocity (m/s)**	**Sphere invert embedment depth (m)**
1	2	5.04	0.611
2	3	0.00	0.076
3	15	5.14	0.653
4	9	6.05	0.812
5	4.5	3.95	0.408
6	15	5.84	0.740
7	9	5.92	0.660
8	4.5	5.62	0.624
9	4.5	5.82	0.702
10	20	6.20	0.782
11	15	5.70	0.670
12	15	5.92	0.630
13	3	5.15	0.610
14	2	4.45	0.580
15	1	3.99	0.569

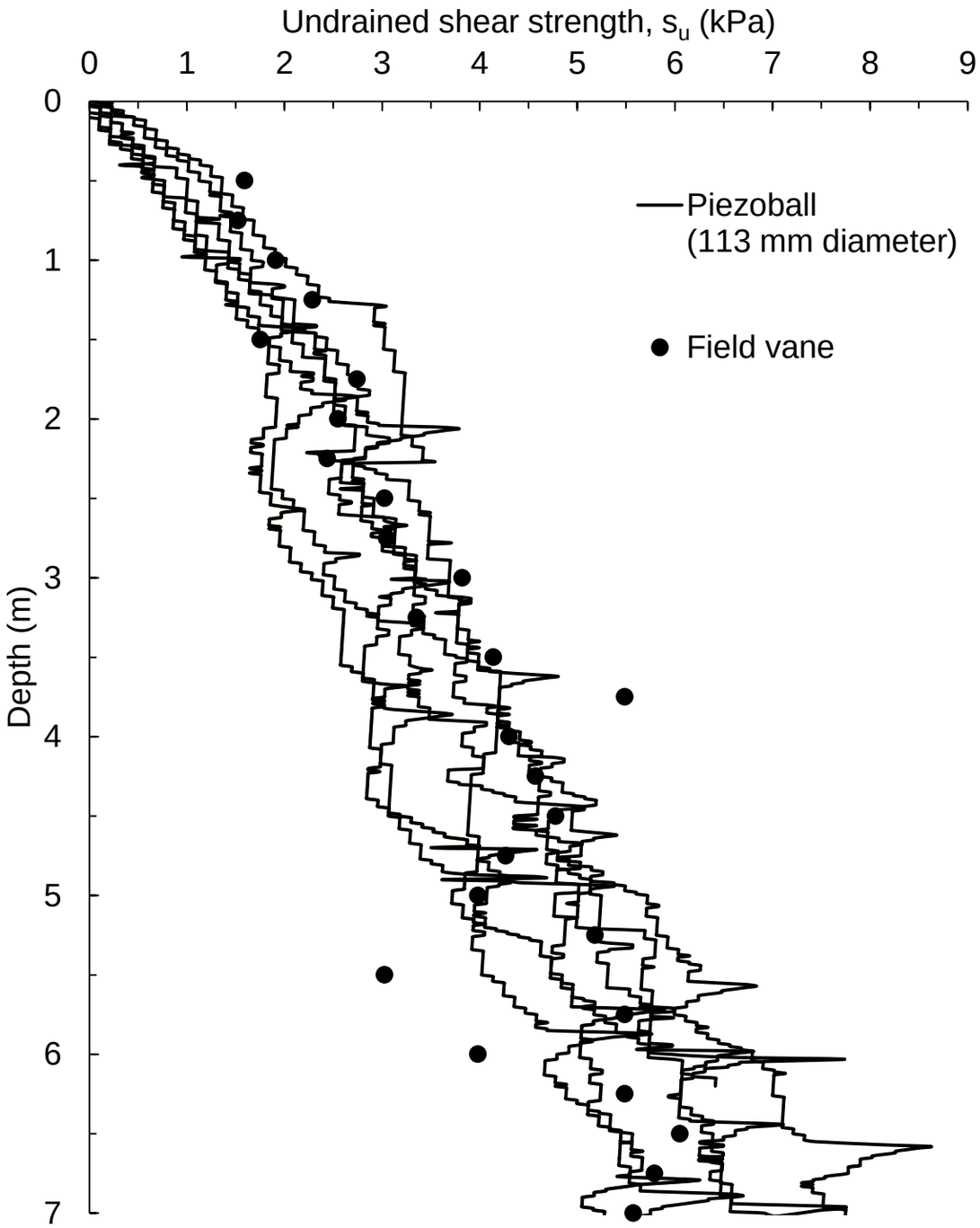
Undrained shear strength, s_u (kPa)
0
1
2
3
4
5
6
7
8
9
Depth (m)
0
1
2
3
4
5
6
7
Piezoball
(113 mm diameter)
Field vane

(a)

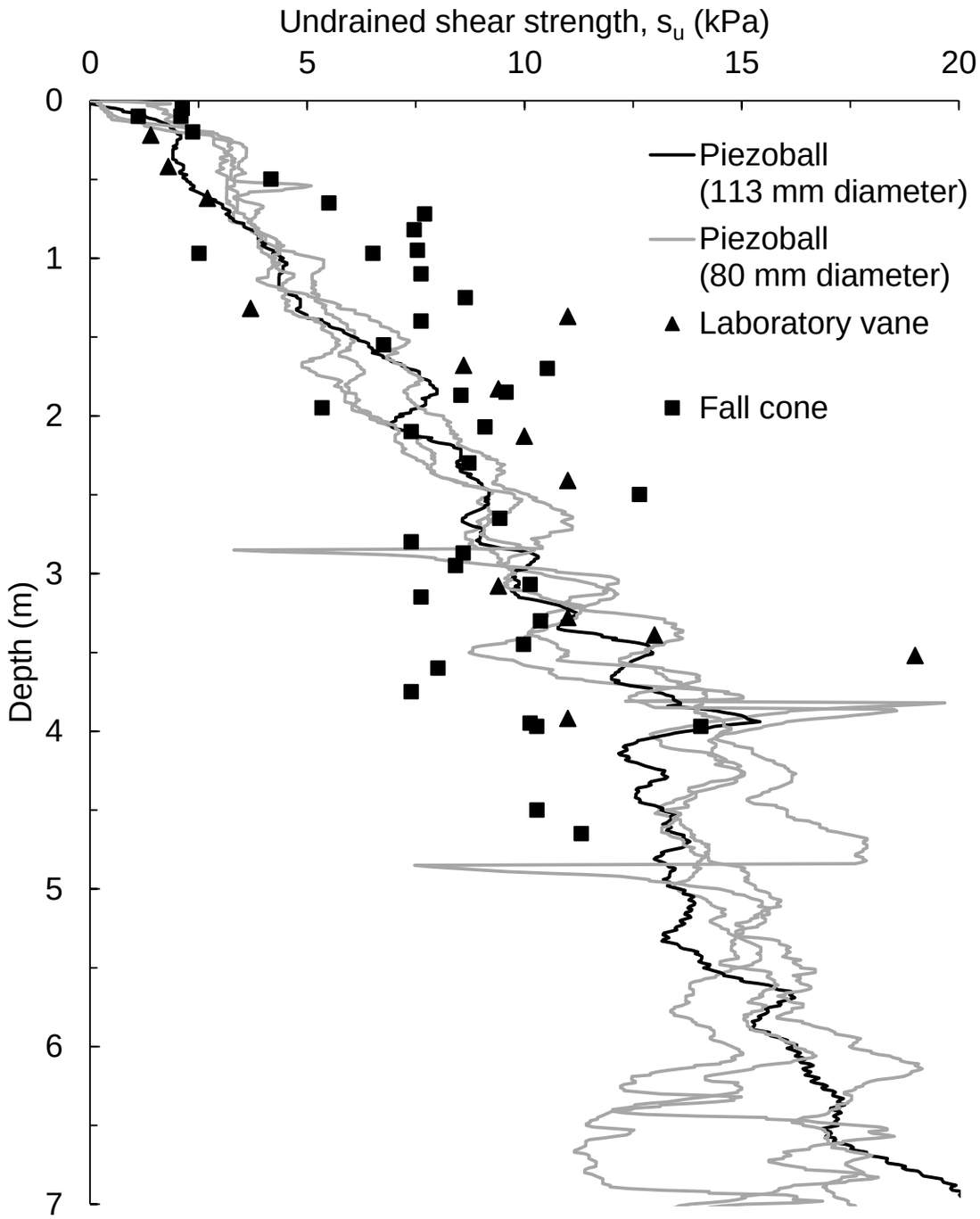
Undrained shear strength, s_u (kPa)
0
5
10
15
20
Depth (m)
0
1
2
3
4
5
6
7
Piezoball
(113 mm diameter)
Piezoball
(80 mm diameter)
Laboratory vane
Fall cone

(b)


(a)


(c)
EPSILON

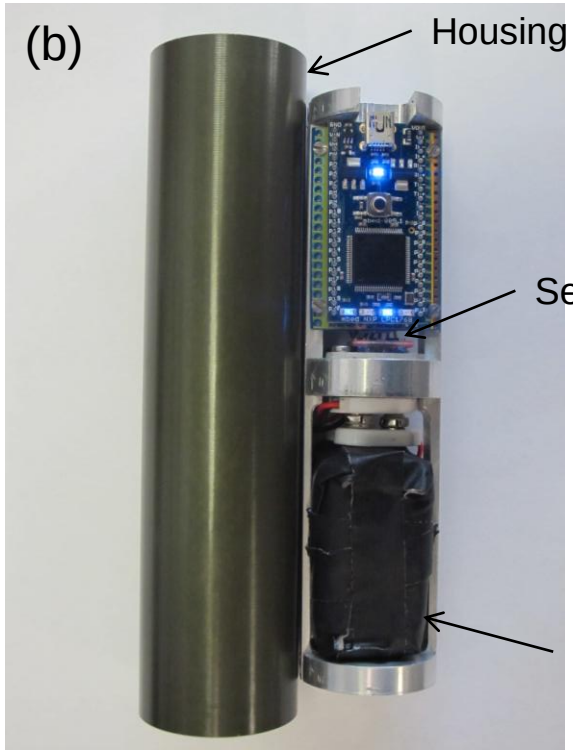
(b)
Housing
Sensors
Batteries

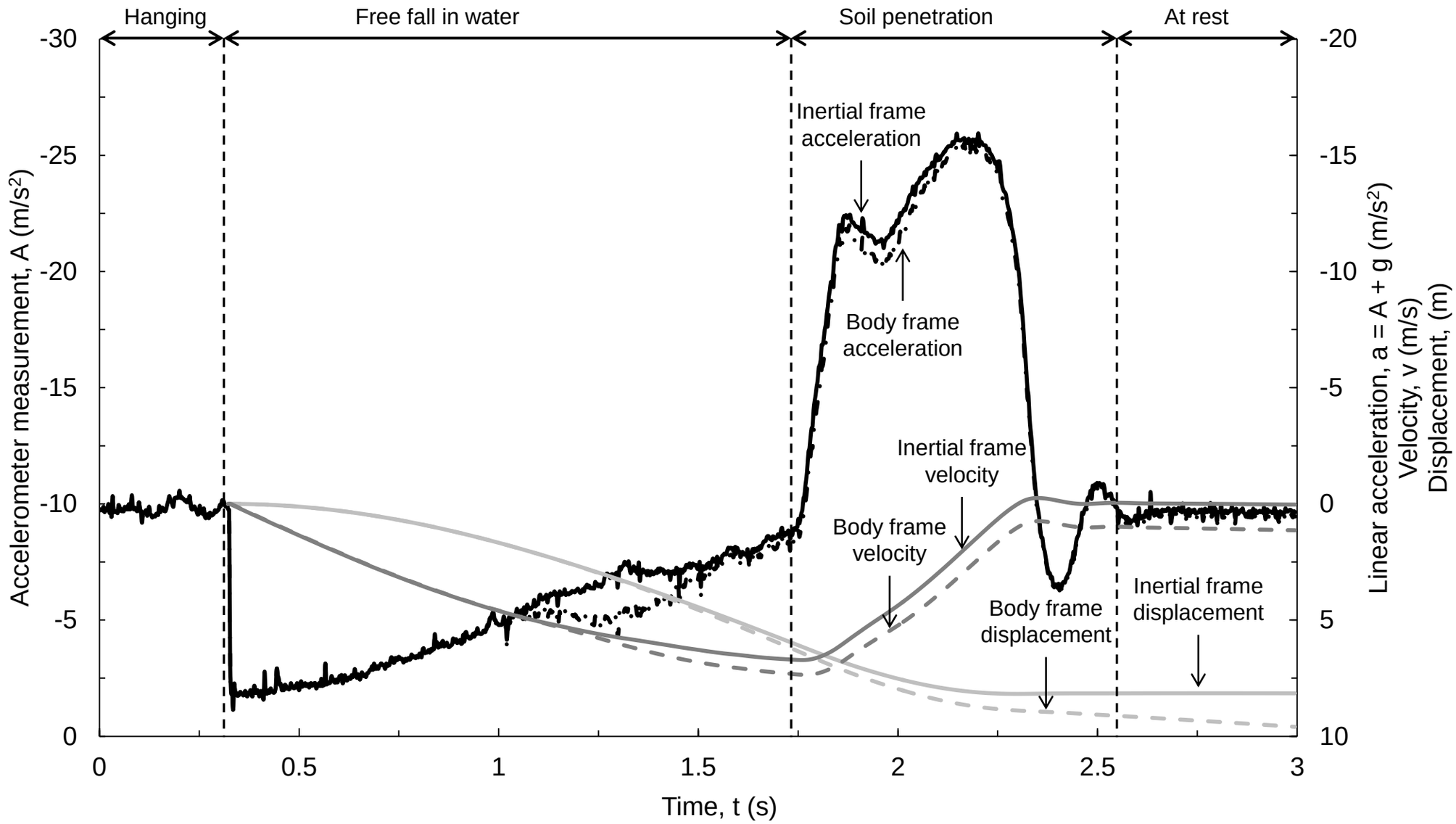
Hanging
Free fall in water
Soil penetration
At rest
Inertial frame acceleration
Body frame acceleration
Inertial frame velocity
Body frame velocity
Body frame displacement
Inertial frame displacement
Accelerometer measurement, A (m/s²)
Linear acceleration, a = A + g (m/s²)
Velocity, v (m/s)
Displacement, (m)
Time, t (s)
-30
-25
-20
-15
-10
-5
0
-20
-15
-10
-5
0
5
10
0
0.5
1
1.5
2
2.5
3

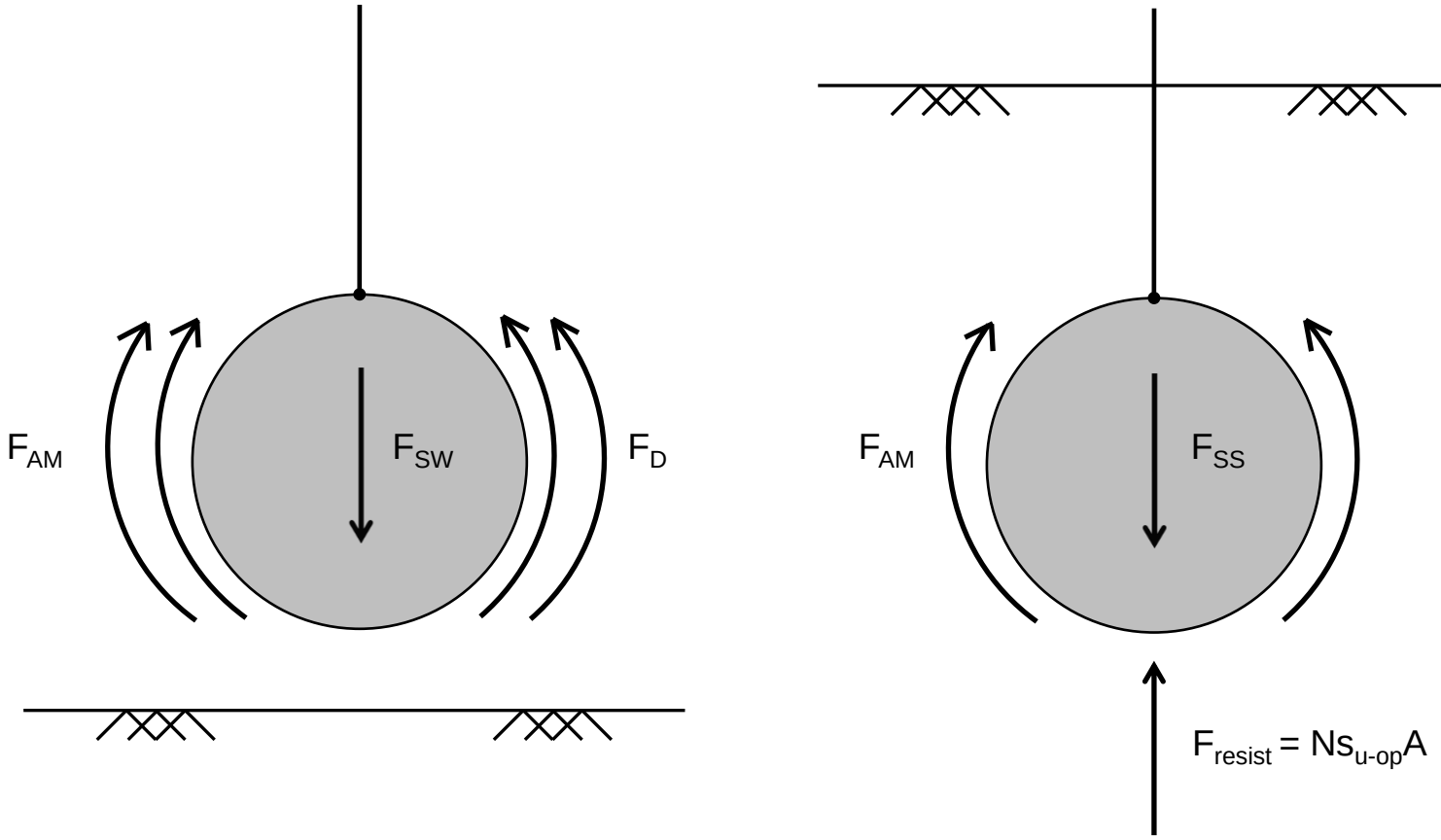

(a) (b)

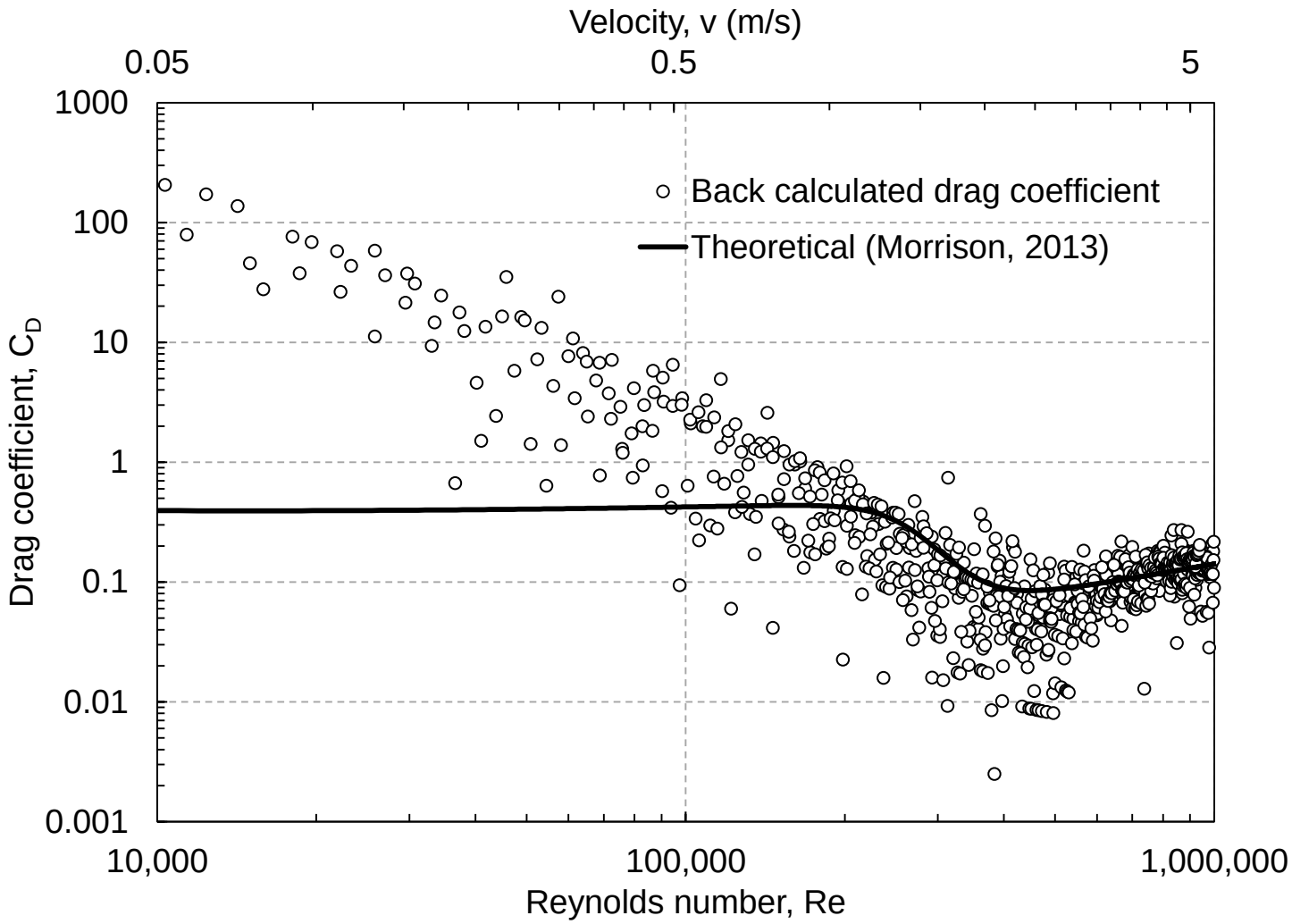
Velocity, v (m/s)
0.05
0.5
5
1000
100
10
1
0.1
0.01
0.001
Drag coefficient, C_D
Back calculated drag coefficient
Theoretical (Morrison, 2013)
10,000
100,000
1,000,000
Reynolds number, Re

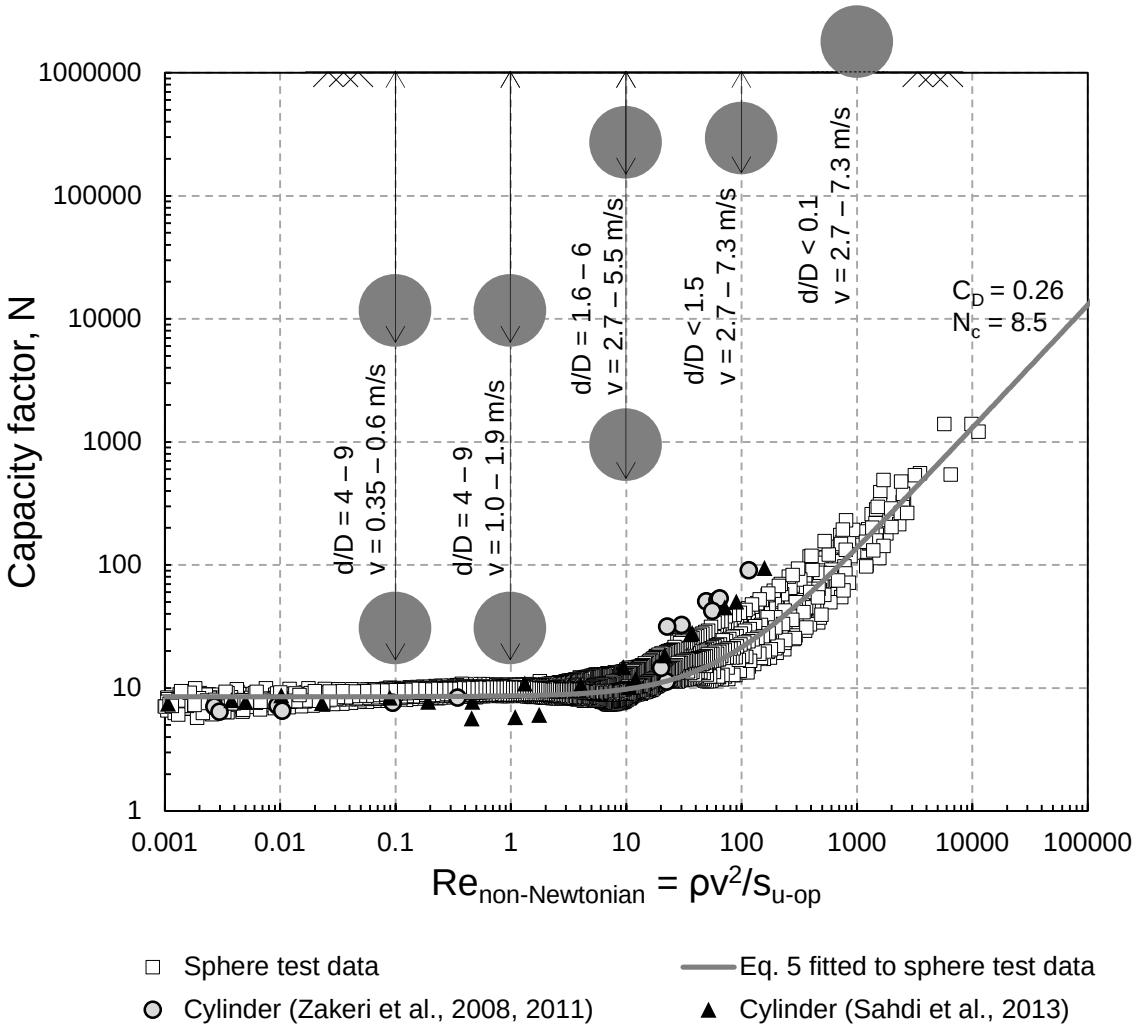
Capacity factor, N
1000000
100000
10000
1000
100
10
1
0.001
0.01
0.1
1
10
100
1000
10000
100000
Re non-Newtonian = ρv²/s u-op
d/D = 4 – 9
v = 0.35 – 0.6 m/s
d/D = 4 – 9
v = 1.0 – 1.9 m/s
d/D = 1.6 – 6
v = 2.7 – 5.5 m/s
d/D < 1.5
v = 2.7 – 7.3 m/s
d/D < 0.1
v = 2.7 – 7.3 m/s
C D = 0.26
N c = 8.5
Sphere test data
Eq. 5 fitted to sphere test data
Cylinder (Zakeri et al., 2008, 2011)
Cylinder (Sahdi et al., 2013)

(a)

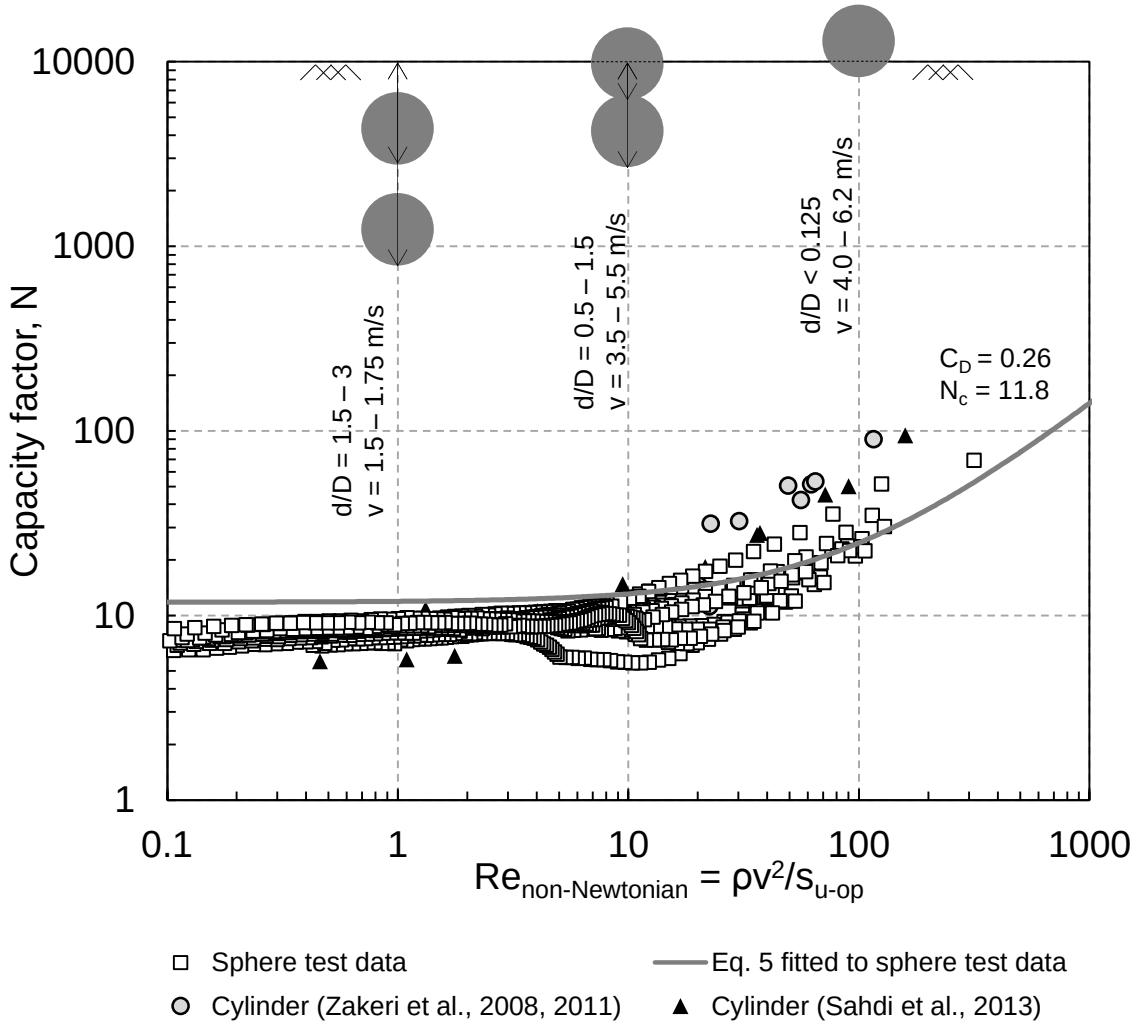
Capacity factor, N
10000
1000
100
10
1
0.1
1
10
100
1000
Re non-Newtonian = ρv²/s u-op
d/D = 1.5 – 3
v = 1.5 – 1.75 m/s
d/D = 0.5 – 1.5
v = 3.5 – 5.5 m/s
d/D < 0.125
v = 4.0 – 6.2 m/s
C D = 0.26
N c = 11.8
Sphere test data
Eq. 5 fitted to sphere test data
Cylinder (Zakeri et al., 2008, 2011)
Cylinder (Sahdi et al., 2013)

(b)

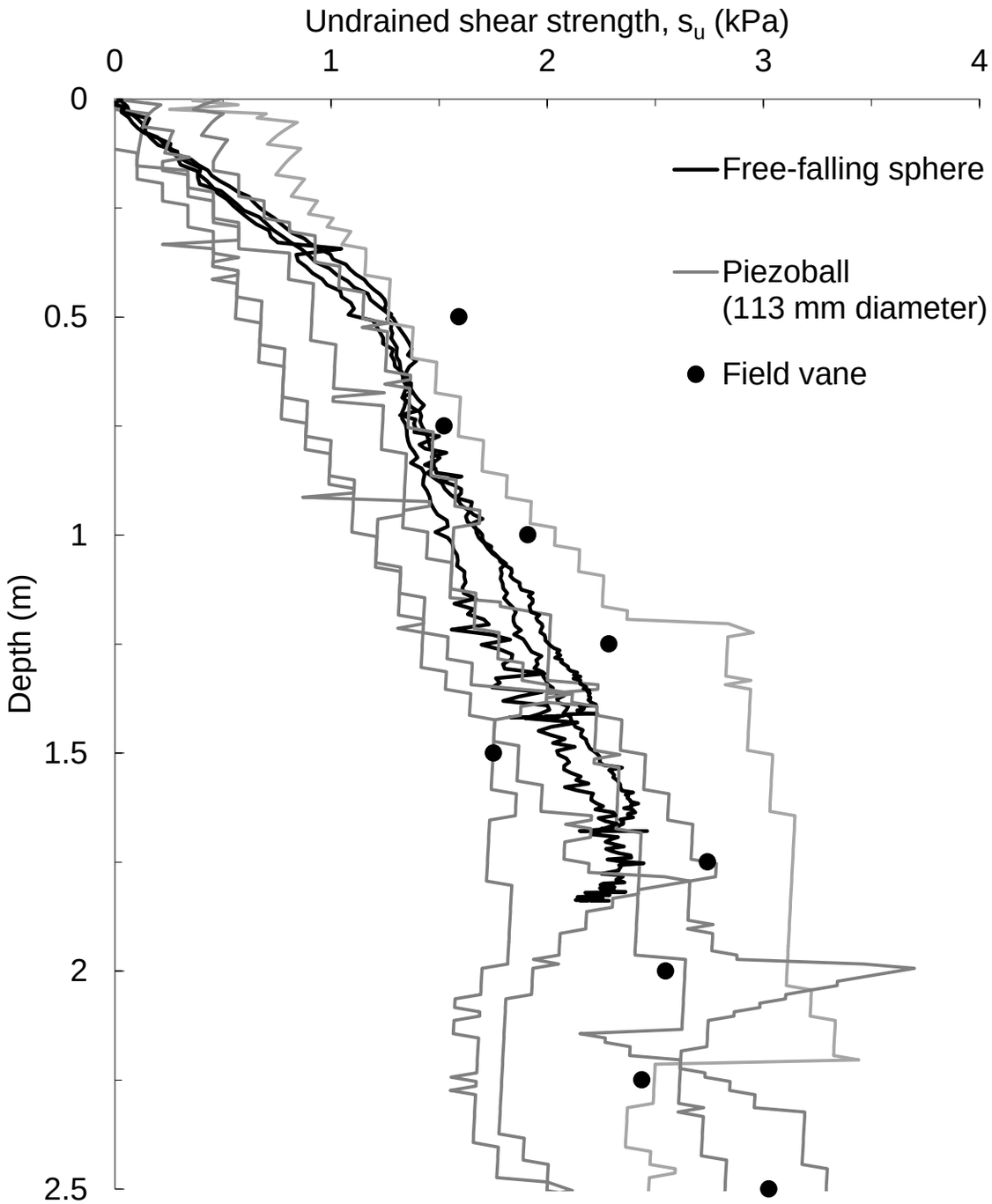
Undrained shear strength, s_u (kPa)
0
1
2
3
4
Depth (m)
0
0.5
1
1.5
2
2.5
Free-falling sphere
Piezoball
(113 mm diameter)
Field vane

(a)

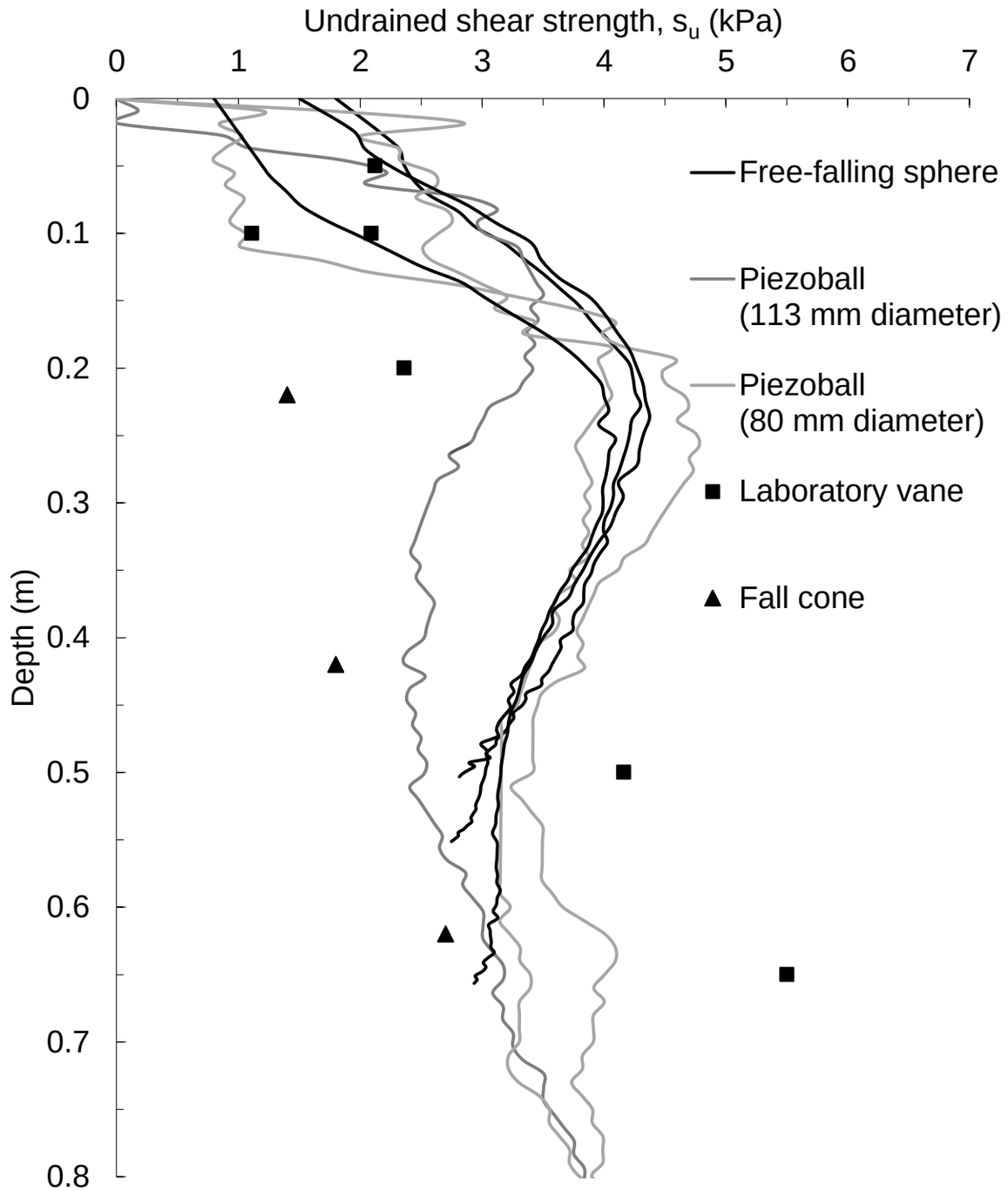
Undrained shear strength, s_u (kPa)
0
1
2
3
4
5
6
7
Depth (m)
0
0.1
0.2
0.3
0.4
0.5
0.6
0.7
0.8
Free-falling sphere
Piezoball
(113 mm diameter)
Piezoball
(80 mm diameter)
Laboratory vane
Fall cone

(b)